Rock Mechanics and Rock Engineering (2023) 56:4629–4645
https://doi.org/10.1007/s00603-023-03266-7

ORIGINAL PAPER

Variable Parameter Creep Model Based on the Separation of Viscoelastic and Viscoplastic Deformations

Wenbo Liu[1,2] · Hui Zhou[1,2] · Shuguang Zhang[3,4] · Chengwei Zhao[1,2]

Received: 2 March 2022 / Accepted: 13 February 2023 / Published online: 22 March 2023

Abstract

The MTS815.02 rock test system is used for performing triaxial compression creep experiments on sandstone to reveal the rheological properties of the rock in deep roadways. Instantaneous elastic, viscoelastic, and viscoplastic strains are separated, and the relationship between the model parameters and the stress and time is established by combining the characteristics of the creep curve. According to non-linear rheological theory, the constitutive equation of a creep model of the rock under a three-dimensional stress state is deduced, and the validity of the model is verified by the experimental data. Results show that the improved creep model comprehensively considers instantaneous elastic, non-linear viscoelastic, and viscoplastic strains, making the theoretical curve of the model highly consistent with the experimental curve. The model can describe the non-linear creep during the loading of sandstone. It can also reflect the creep parameters during the deformation. The correlation coefficients of the experimental curve and the theoretical curve under the same stress are both greater than 0.90. The comparison results verify the validity and feasibility of the creep model.

Highlights

- According to the characteristics of creep curve, the instantaneous strain, viscoelastic strain and viscoplastic strain are separated.
- The creep model based on viscoelastic-plastic strain separation can well describe the accelerated creep characteristics of rock creep process.
- The variation of creep parameters also reflects the evolution process of damage accumulation and deterioration of material properties.

✉ Hui Zhou
hzhou@whrsm.ac.cn

✉ Shuguang Zhang
fx5152@126.com

Wenbo Liu
15393162288@163.com

[1] State Key Laboratory of Geomechanics and Geotechnical Engineering, Institute of Rock and Soil Mechanics, Chinese Academy of Sciences, Wuhan 430071, Hubei, China

[2] University of Chinese Academy of Sciences, Beijing 100049, China

[3] Guangxi Key Laboratory of Geomechanics and Geotechnical Engineering, Guilin 541004, China

[4] School of Civil Engineering, Guilin University of Technology, Guilin 541004, China

Keywords Rheological properties · Surrounding rock · Instantaneous elastic strain · Non-linear viscoelastic strain · Viscoplastic strain · Non-linear

Abbreviations

σ_1	Axial stress
ε_e	Instantaneous strain
K_e	Bulk modulus at the instantaneous strain stage
σ_m	Spherical tensor of stress
a_i	Fitting parameter

c_i Fitting parameter
σ_A Critical damage stress
η_{ve} Viscosity coefficient of the viscoelastic body
G_{vei} Shear modulus at any time
A_i Value of parameter A at any time
S_{11} Stress tensor
ε_{vp} Strain of the Newton's dashpot
ε_{nl} Strain of the non-linear dashpot
t^* Time to enter the accelerated creep
σ_3 Radial stress
G_e Shear modulus at the instantaneous strain stage
ε_m Spherical tensor of strain
ε_V Volumetric strain
b_i Fitting parameter
ε Total creep strain
ε_{ve} Viscoelastic strain
G_{ve} Shear modulus of the viscoelastic body
η_{vei} Viscosity coefficient at any time
η_{nl} Viscosity coefficient of the non-linear dashpot
$g(\cdot)$ A function
η_{vp} Viscosity coefficient of the Newton's dashpot
t_i Different time point
σ_S Long-term strength

1 Introduction

The mechanical properties of rock creeps are one of the inherent rock properties. In particular, soft rocks with complex conditions in deep geological environments are affected by high in situ stress, high temperature, and high water pressure (Cornet et al. 2018). The joints and fissures are often well developed, showing considerable creep from the macroscopic view. This deformation characteristic is critical to the safety and long-term stability of a structure with a long service life (Andargoli et al. 2019). The influencing factors include high temperature, high ground stress, high seepage and strong disturbance. At present, the research on rock creep characteristics mainly includes laboratory uniaxial and triaxial loading compression creep test research and theoretical research on establishing the corresponding element (elastic element, viscous element, and plastic element), comprising a combined model based on the test results (Brantut et al. 2013). However, each parameter in the model is identified only through the overall fitting of the creep curve (Zhou et al. 2011; Tomanovic et al. 2006). The obtained variation of model parameters is difficult to objectively reflect the real variation of the whole process of rock creep (Tang et al. 2018; Li et al. 2007; Diisterloh et al. 2013).

Yang et al. (2018) replaced the viscous elements in the traditional Nishihara model with fractional elements with respect to time and stress changes to create a new model that describes rock accelerated creep. The correctness of the model was verified by experimental data fitting. Wang et al. (2018a) studied the unloading creep characteristics of layered rock samples of Jinping II Hydropower Station and obtained the creep curves under different confining pressures. They also established non-linear creep model constitutive equation under three-dimensional stress state. The creep parameters were identified by an optimization algorithm, and the creep parameters were non-linearly degraded as the confining pressure decreased. The combined creep model of Maxwell and Hooke models was established based on acoustic emission technology, and the elastic and viscous parameters of the model were calculated. The proposed model can accurately predict the stress–strain response of rock salt under loading and unloading conditions (Singh et al. 2018). A new non-linear creep damage model was proposed by considering the influence of initial damage on the creep properties of rock. The parameters of the non-linear creep damage model were obtained by fitting, and the correctness of the creep characteristics of the sandstone under different initial damage conditions was verified (Hou et al. 2019). A curve of sandstone creep was described by a non-linear and nonstationary plastic viscosity (NNPV) creep model. The rock creep parameters at three pressure levels were determined. The theoretical curves using the NNPV model agree well with the experimental data (Wang et al. 2018b). The fitting of the creep parameters does not have an obvious physical meaning.

In this article, the author believe that the establishment of the rock creep model still needs to be perfected by analyzing and summarizing the above research results and the current development process of rock creep mechanics. At present, the most mature and widely used rock creep model theory is the component combination model. This model combines elastic elements, viscous elements and plastic elements through different series and parallel relations to reflect the creep characteristics of rocks under different stresses. However, all traditional creep models cannot describe accelerated creep under high stress. Combined with the characteristics of the rock creep curve, long-term strength is used as the stress threshold of viscoplastic creep. The instantaneous strain, viscoelastic strain, and viscoplastic strain are analyzed. The functional relationship between each creep parameter and stress and time is established through numerical fitting. A correction coefficient is introduced to optimize the creep model. A variable parameter creep model that can describe the accelerated creep is proposed and expected to provide references for the design of rock support and long-term stability evaluation of roadways.

2 Laboratory Testing of Rocks

2.1 Determination of Critical Damage Stress

The rocks used in this study are all taken from a mining area in Liaoning. The rock is at a depth of about 400 m. The actual measurement shows that the maximum horizontal in situ stress value of the surrounding rock at this position can reach about 13.36 MPa. Therefore, the confining pressure is set as 10 and 15 MPa. In order to eliminate the variability of rock samples, it is necessary to ensure that the creep test needs to be taken from the same rock mass. Rock samples with obvious external defects are rejected. Under each confining pressure, three rock samples are used to carry out mechanical properties tests. When the difference between the peak strength of the three rock samples is greater than 15%, the mechanical properties test under this condition needs to be carried out again. When the difference between the peak strength of the three rock samples is less than 15%, the average value of the peak strength of the three rocks is taken as the peak strength value of this test. The method of determining the critical damage stress of rock is shown in Fig. 1 (confining pressure 15 MPa) (Liu et al. 2021).

The phenomenon of rock dilatancy is accompanied by the initiation of microcracks (Heap et al. 2009). The expansion of microcracks marks the damage inside the rock. If the stress of the rock is constant, the microcracks will continue to develop with time under the action of long time. The final sample will be damaged. When the microcracks appear in the rock, the radial deformation growth rate of the rock is greater than the axial deformation growth rate. Therefore, the volumetric strain rate

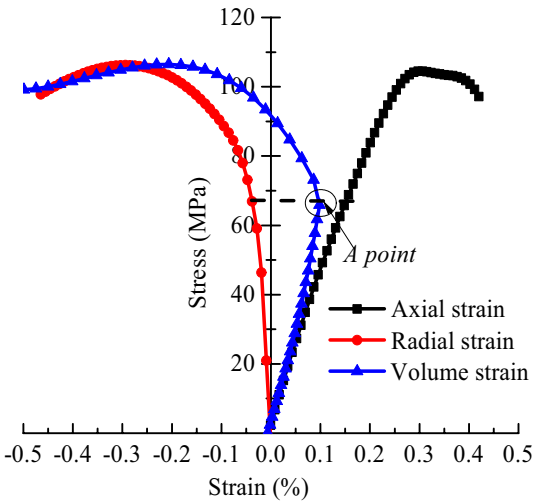

Fig. 1 Method for determining critical damage stress of rock

begins to slow down on the stress–volume strain curve. The volume strain curve develops in the opposite direction and there will be an inflection point. The inflection point of the volumetric strain curve is used to determine the point as a sign of the occurrence of microcracks inside the rock. Zhang et al. (2019) define the inflection point (point A) as the critical point of rock damage. Therefore, when the creep stress is less than the damage critical stress, Eq. (1b) is established. When the creep stress is less than the damage critical stress, Eqs. (1c) and (1d) are established. Figure 1 shows that the critical point stress σ_A of the rock under a confining pressure of 15 MPa is 65.48 MPa. For the convenience of calculation, the critical damage stress is set as 65 MPa.

2.2 Triaxial Creep Test of Rock

Triaxial creep test is carried out by using creep test method of single sample loaded separately. Combined with the previous experimental results of rock creep and the long period of creep test, a rock samples for creep are performed under each stress condition. Under the confining pressure of 10 MPa, the number of creep test samples is 9. The axial stresses are 35, 40, 45, 50, 55, 60, 65, 70, and 75 MPa. Under the confining pressure of 15 MPa, the number of creep test samples is 10. The axial stresses are 50, 55, 60, 65, 70, 75, 80, 85, 90, and 95 MPa. When the measured axial deformation of the sample is not greater than 0.001 mm within 2 h, it can be considered that the creep rate of rock no longer changes. At this time, the creep strain is considered stable. The creep test can apply the next load level and repeat the cycle until accelerated creep failure of the rock occurs. The creep characteristics of a single sample loaded individually (a new sample is used for each creep stage) are not affected by the historical load. They are related to the characteristics of the rock and test conditions (Zhang et al. 2021). Therefore, the data can be used directly without processing.

The axial creep test curves under different confining pressure are shown in Fig. 2 (Zhang et al. 2019). Figure 2 shows that the instantaneous strain is related to the applied stress level. The instantaneous strain increases as the stress increases. A linear relation exists between the instantaneous strain and stress level. The percentage of instantaneous strain to the total strain shows a trend of first increase, decrease and then increase. This is due to the presence of certain pores in the sandstone. The pores of the sandstone are compressed at the initial moment of loading. After the pores are completely compacted, the sandstone undergoes a large number of cracks, leading to a large initial instantaneous strain of the sandstone and a small subsequent instantaneous strain (the deformation provided by fracture deformation is much smaller than the deformation provided

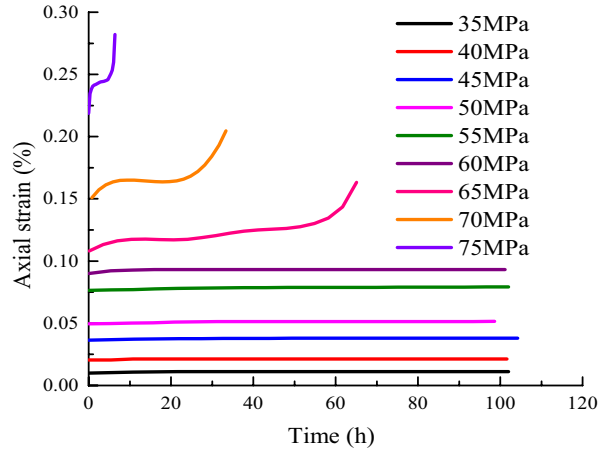

(a)Axial creep-time curve under $\sigma_3 = 10$ MPa

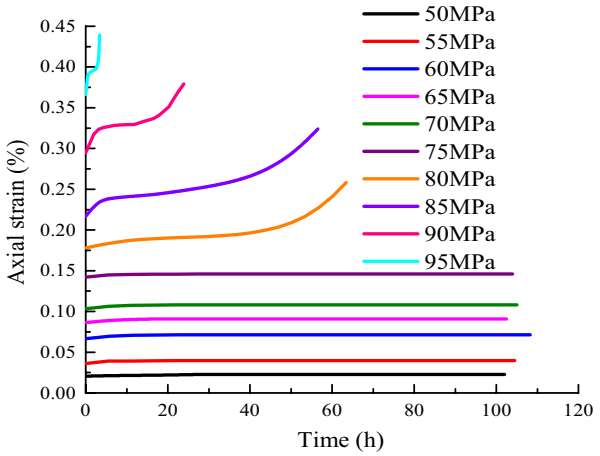

(b)Axial creep-time curve under $\sigma_3 = 15$ MPa

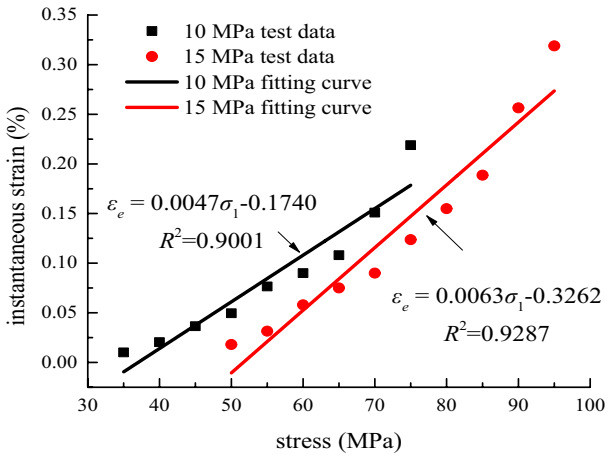

(c)Relationship between instantaneous strain and stress

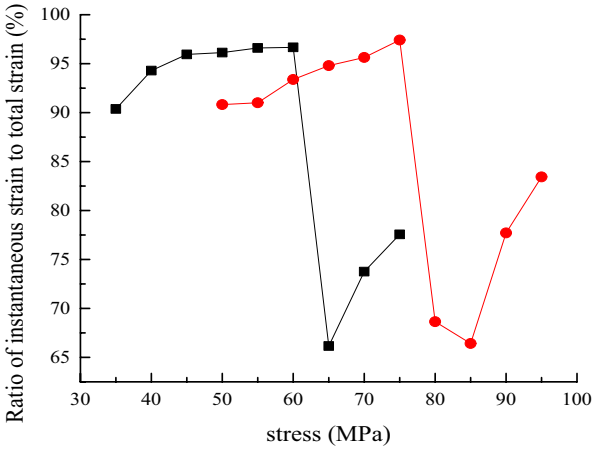

(d)The relationship between instantaneous strain and total strain and stress

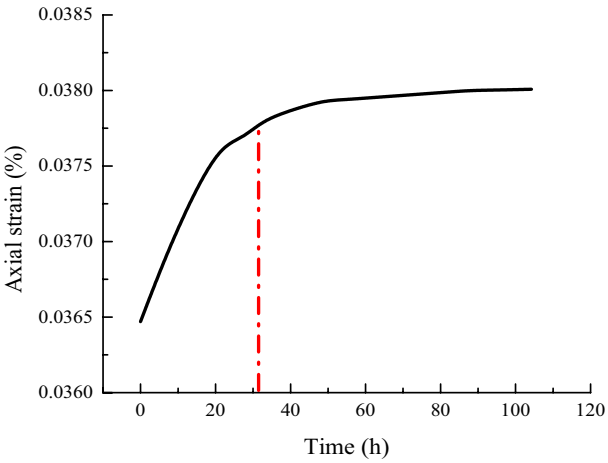

(e) $\sigma_1 = 45$ MPa

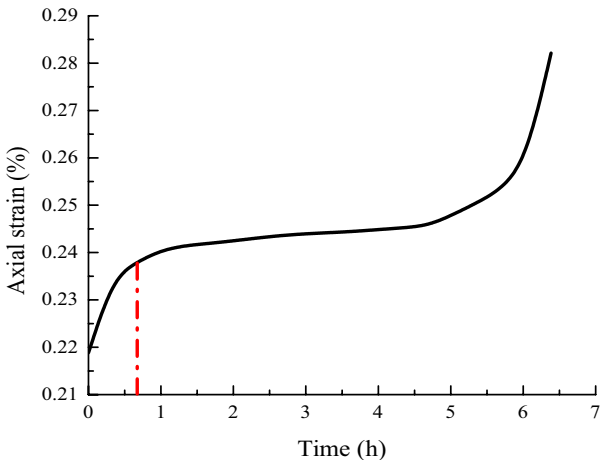

(f)$\sigma_1 = 75$ MPa

Fig. 2 Axial creep time curve under different confining pressures

by pore compression). The accelerated creep duration gradually decreases as the stress level increases. This finding indicates that the increase in stress aggravates the internal damage development and the expansion of cracks in the sandstone. When the applied load is greater, the initial creep time of the rock is shorter. The above phenomenon is explained by the creep curve with a confining pressure of 10 MPa. The rock primary creep time is 32.62 h when the axial stress is 45 MPa. However, the rock primary creep time is only 0.67 h when the axial stress is 75 MPa (Hu et al. 2018).

2.3 Determination of Long-Term Strength

The long-term strength of the rock can be determined according to the isochronous stress–strain method (Shen et al. 2011). The isochronous curve refers to the relationship between the creep and the corresponding stress at the same time in a set of creep curves for different stress levels. The isochronous curve method transforms the straight line of each isochronous line into a curve. The stress corresponding to the asymptote formed by the yield stress is similar to the long-term strength of the rock. The inflection point of the isochronous curve marks the transition of rock from the viscoelastic stage to the viscoplastic stage. The internal structure of the rock changes and begins to break down. The isochronous curve method is one of the methods to determine the long-term strength of rock. This method has been introduced into the relevant rock mechanics test specifications. The isochronous stress–strain curve data of rock is calculated according to the axial creep–time curve. The axial isochronous stress–strain curve is drawn by taking the confining pressure of 15 MPa as an example. This study selects the time as 5, 10, 20, 40, 60, 80, and 100 h.

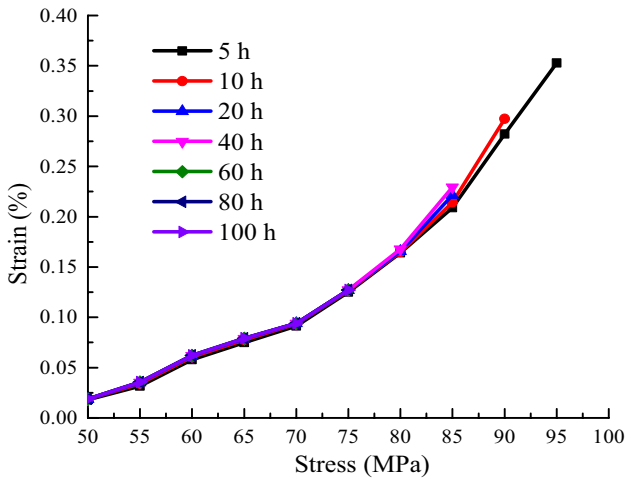

Fig. 3 Axial isochronous stress–strain curve

Figure 3 shows that the isochronous stress–strain curves overlap before the stress reaches 80 MPa. However, the isochronous stress–strain curve begins to diverge after the stress value reaches 80 MPa. The stress value corresponding to the inflection point can be used as the long-term strength of the rock (Shen et al. 2011). In particular, the long-term strength value of the rock is 80 MPa when the confining pressure is 15 MPa.

3 Establishment of the Rock Non-linear Creep Model

3.1 Division of Creep Curve

The rock deformation under external load mainly includes instantaneous strain, primary creep strain, steady-state creep strain, and accelerated creep strain (Yu et al. 2016). It can be seen from Fig. 4 that the creep curve can be divided into four parts. The Newton's dashpot cannot describe the accelerated creep of rock. Therefore, this paper refers to the non-linear dashpot to describe the accelerated creep of rock. Under a three-dimensional stress state, the creep equation of the non-linear dashpot is (Qi et al. 2012)

$$\varepsilon_{nl} = \frac{\sigma_1 - \sigma_3}{6\eta_{nl}}(t - t^*)^2, \varepsilon \geq \varepsilon_a \tag{1a}$$

where σ_1 is the axial stress, σ_3 is the radial stress, ε_{nl} is the strain of the non-linear dashpot, ε_a is the strain at the start

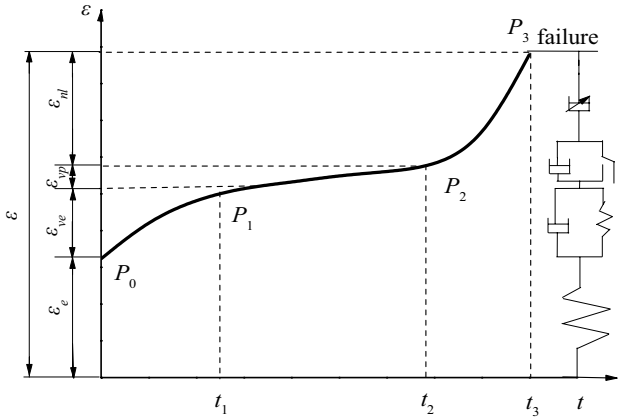

Fig. 4 Relationship between rock creep curve and improved creep model. ε is the strain, ε_e is the instantaneous strain, ε_{ve} is the decay strain, ε_{vp} is the stable strain, ε_{nl} is the accelerated strain, t is the time, t_1 is the start time of stable creep, t_2 is the start time of accelerated creep, t_3 is the creep failure time, P_0 is the demarcation point between decay creep and instantaneous deformation, P_1 is the demarcation point between decay creep and stable creep, P_2 is the demarcation point between accelerated creep and stable creep, P_3 is the end point of creep failure

of a non-linear dashpot, η_{nl} is the viscosity coefficient of the non-linear dashpot, t^* is the time to enter the accelerated creep, which can be obtained from the test curve. It refers to the boundary between steady creep and accelerated creep.

According to the corresponding relationship between the model and the creep curve in Fig. 4, the Nishihara model is connected in series with the non-linear dashpot to obtain a model that can describe the accelerated creep. Therefore, the Eq. (1a) is combined with the creep equation of Nishihara model, and the equation of the modified creep model are (1b)–(1d).

When $\sigma < \sigma_A$, $\varepsilon < \varepsilon_a$

$$\varepsilon = \frac{\sigma_1 + 2\sigma_3}{9K_e} + \frac{\sigma_1 - \sigma_3}{3G_e} + \frac{\sigma_1 - \sigma_3}{3G_{ve}}\left[1 - \exp\left(-\frac{G_{ve}}{\eta_{ve}}t\right)\right]. \tag{1b}$$

When $\sigma \geq \sigma_A$, $\sigma \geq \sigma_S$ and $\varepsilon < \varepsilon_a$

$$\varepsilon = \frac{\sigma_1 + 2\sigma_3}{9K_e} + \frac{\sigma_1 - \sigma_3}{3G_e} + \frac{\sigma_1 - \sigma_3}{3G_{ve}}\left[1 - \exp\left(-\frac{G_{ve}}{\eta_{ve}}t\right)\right] + \frac{\sigma_1 - \sigma_3 - \sigma_s}{3\eta_{vp}}t. \tag{1c}$$

When $\sigma \geq \sigma_S$ and $\varepsilon \geq \varepsilon_a$

$$\varepsilon = \frac{\sigma_1 + 2\sigma_3}{9K_e} + \frac{\sigma_1 - \sigma_3}{3G_e} + \frac{\sigma_1 - \sigma_3}{3G_{ve}}\left[1 - \exp\left(-\frac{G_{ve}}{\eta_{ve}}t\right)\right] + \frac{\sigma_1 - \sigma_3 - \sigma_s}{3\eta_{vp}}t + \frac{\sigma_1 - \sigma_3}{6\eta_{nl}}(t - t^*)^2, \tag{1d}$$

where σ_1 is the axial stress, σ_3 is the radial stress, G_e is the shear modulus at the instantaneous strain stage, K_e is the bulk modulus at the instantaneous strain stage, η_{ve} is the viscosity coefficient of the viscoelastic body, G_{ve} is the shear modulus of the viscoelastic body, η_{vp} is the viscosity coefficient of the Newton's dashpot.

3.2 Establishment of the Instantaneous Strain Model

Due to the single sample creep loading method, the instantaneous strain of the rock cannot be separated into instantaneous elastic strain (the elastic strain refers to the strain that can be recovered after the stress is completely removed) and instantaneous plastic strain (the instantaneous plastic strain refers to the strain that remains in a material element after the stress has completely disappeared). For the convenience of calculation, it is assumed here that all the instantaneous strains of the rock are instantaneous elastic strains (Zhao et al. 2017a).

The Hooke model can describe the deformation of the rock in the instantaneous elastic strain stage. The instantaneous elastic strain of the rock can be expressed as (Xu et al. 2018b; Zhou et al. 2010)

$$\varepsilon_e = \frac{\sigma_1 + 2\sigma_3}{9K_e} + \frac{\sigma_1 - \sigma_3}{3G_e}, \tag{2a}$$

where σ_1 is the axial stress, σ_3 is the radial stress, ε_e is the instantaneous strain, G_e is the shear modulus at the instantaneous strain stage, and K_e is the bulk modulus at the instantaneous strain stage.

At the instantaneous strain stage, the bulk modulus K_e can be expressed as Eq. (2b) (Findley et al. 1976).

$$K_e = \frac{\sigma_{\mathrm{m}}}{3\varepsilon_{\mathrm{m}}} = \frac{\sigma_{\mathrm{m}}}{\varepsilon_{\mathrm{V}}}, \tag{2b}$$

where σ_{m} is the spherical tensor of stress, ε_{m} is the spherical tensor of strain(Liu et al. 2022), and ε_{V} is the volumetric strain.

The shear modulus at the instantaneous strain stage can be obtained by substituting Eq. (2b) into Eq. (2a) (Huang et al. 2011; Munson et al. 1993)

$$G_e = \frac{3K_e(\sigma_1 - \sigma_3)}{9K_e\varepsilon_e - (\sigma_1 + 2\sigma_3)}. \tag{2c}$$

According to the axial creep test curve, the change of the instantaneous strain of the rock under different stresses is shown in Fig. 5 (with 15 MPa confining pressure taken as an example). The shear modulus and bulk modulus of the instantaneous strain stage are calculated by combining Eqs. (2a), (2b) and (2c) and the instantaneous strain of the rock under different stresses. The shear modulus in the instantaneous strain stage is only affected by stress. It is not related to the creep time. However, the variation rules of bulk modulus

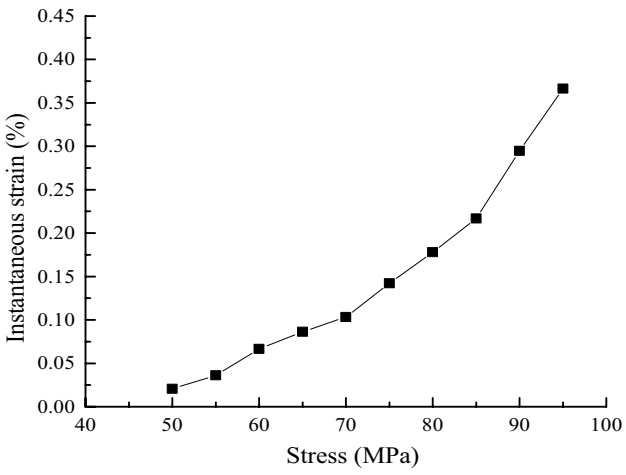

Fig. 5 Variation of rock instantaneous strain under different axial stresses and at confining pressure of 15 MPa

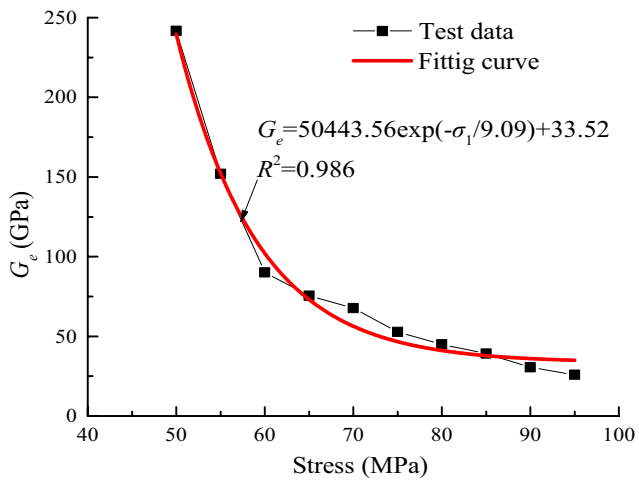

(a)The relationship between G_e and stress

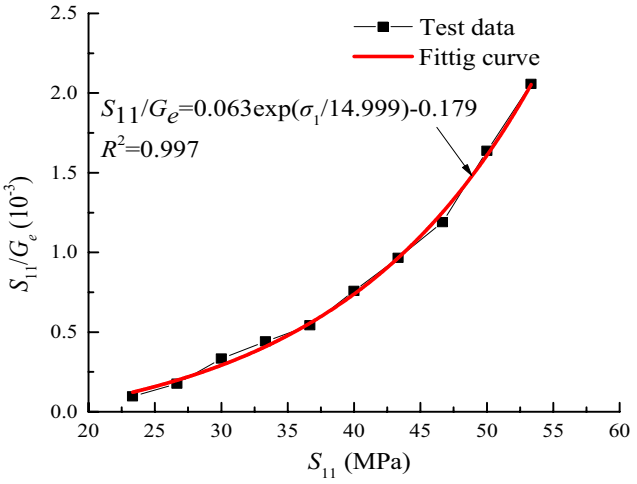

(b)The relationship between S_{11}/G_e and S_{11}

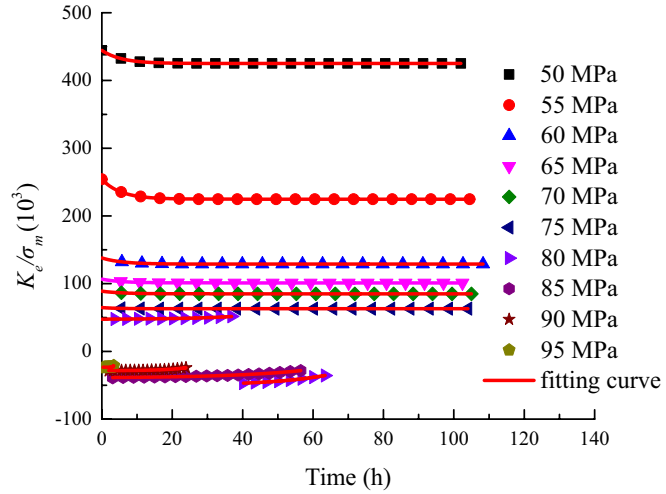

(c)The relationship between K_e/σ_m and time under stress level 50, 55, 60, 65, 70, 75, 85, 90, 95 MPa

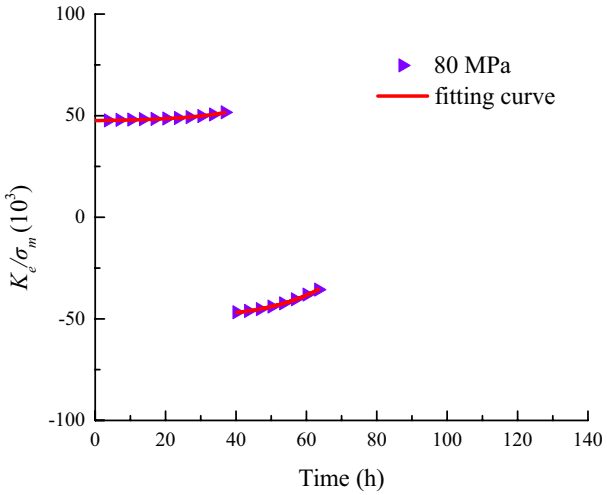

(d)The relationship between K_e/σ_m and time under an axial stress 80 MPa

Fig. 6 The relationship between G_e, S_{11}/G_e, K_e/σ_m and stress in the instantaneous strain stage

under different stresses are quite different because the bulk modulus is positive when the stress is less than 80 MPa. The bulk modulus is negative when the stress exceeds 80 MPa. But describing the relationship of bulk modulus to stress and time with a unified mathematical model is difficult. Therefore, the relationship of positive and negative bulk modulus values to time and stress must be discussed separately.

The shear modulus and bulk modulus at the instantaneous strain stage can be calculated by substituting the experimental data into Eqs. (2b) and (2c). The relationship between the shear modulus and bulk modulus and stress in the instantaneous strain stage are shown in Fig. 6.

It can be seen from Fig. 6 that the shear modulus of the rock in the instantaneous strain stage shows a decreasing trend with the increase of the applied stress. The shear modulus G_e in the instantaneous strain stage is continuously degraded under the action of stress. The expressions between the shear modulus and bulk modulus and stress in the instantaneous strain stage are as follows.

$$S_{11}/G_e = 0.063\exp\left(\sigma_1/14.999\right) - 0.179, R^2 = 0.997 \quad (3a)$$

$$K_e/\sigma_m = a_1\exp\left(-b_1/x\right) + c_1 \quad (3b)$$

Table 1 The fitting parameters of the bulk modulus K_e

Stress level/MPa Fitting parameters	a_3	b_3	c_3	R^2
50	5.723	1.304	2.842	0.912
55	5.376	1.459	3.468	0.924
60	5.082	1.400	3.426	0.932
65	4.375	1.657	6.283	0.908
70	3.652	2.306	6.431	0.919
75	3.276	2.448	6.722	0.917
80 (positive value)	2.963	2.025	3.682	0.892
80 (negative value)	2.496	1.789	4.162	0.944
85	2.150	2.585	5.504	0.940
90	1.462	3.273	8.355	0.917
95	0.903	3.147	4.252	0.948

$$S_{11} = \frac{2}{3}(\sigma_1 - \sigma_3), \tag{3c}$$

where a_1, b_1, and c_1 are the fitting parameters, S_{11} is the stress tensor.

The fitting parameters are shown in Table 1.

The K_e value represents the expansion and compression state of the rock volume because the bulk modulus directly reflects the change of volume deformation under the action of stress and time. Figure 6 shows that compared with the original volume, the volume of the sample is in a compressed state when the stress is less than 80 MPa. The stress at the demarcation point is selected as 80 MPa, because the bulk modulus changes from positive to negative under the action of the stress value. The volume of the rock sample gradually changes from compression to expansion. The rock gradually changes from a compressed state to an expanded state when the stress exceeds 80 MPa (Yan et al. 2010). The K_e value is reflected in the change from positive to negative. The rock has been in a state of expansion when the stress exceeds 80 MPa (Yan et al. 2009). However, the absolute of the K_e value decreases. This finding shows that the expansion of the rock becomes increasingly obvious.

3.3 Establishment of the Viscoelastic Strain Model

According to the assumptions in Sect. 2, the creep of the rock at 65, 60, 55, and 50 MPa are all the sum of viscoelastic and instantaneous strains. Equation (4) calculates the viscoelastic strain of the rock (Wu et al. 2015; Ma et al. 2013). The viscoelastic strain curve of the rock under the action of four stress levels is Fig. 7.

$$\varepsilon_{ve} = \varepsilon - \varepsilon_e, \tag{4}$$

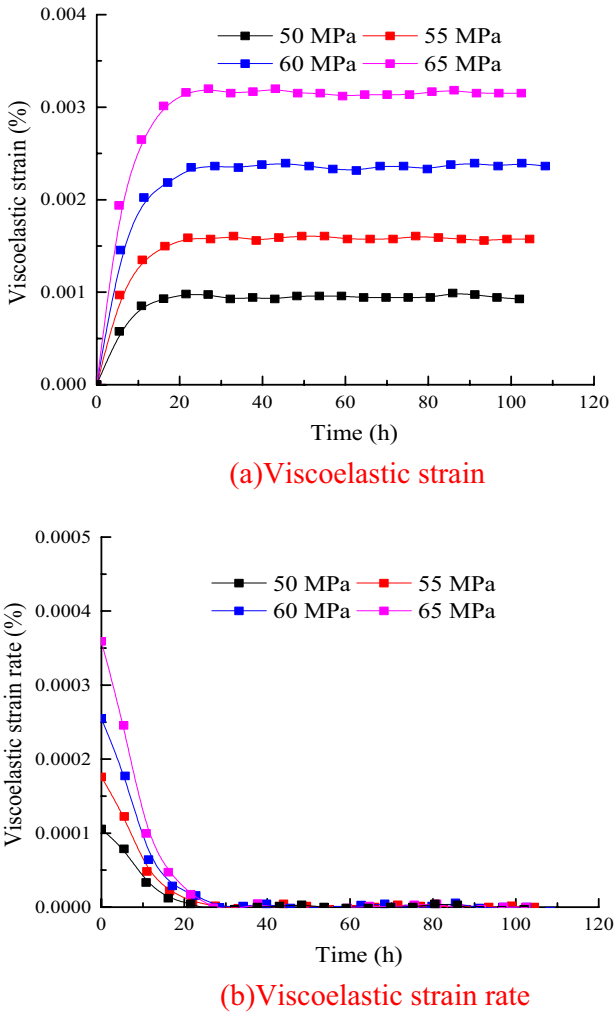

Fig. 7 Viscoelastic strain and viscoelastic strain rate of sandstone under different axial stresses

where ε is the total strain, ε_e is the instantaneous strain, and ε_{ve} is the viscoelastic strain.

In a three-dimensional state, the Kelvin creep model is (Jin et al. 1998; Jing et al. 2018; Xu et al. 2015)

$$\varepsilon_{ve} = \frac{\sigma_1 - \sigma_3}{3G_{ve}}\left[1 - \exp\left(-\frac{G_{ve}}{\eta_{ve}}t\right)\right], \tag{5}$$

where η_{ve} is the viscosity coefficient of the viscoelastic body, and G_{ve} is the shear modulus of the viscoelastic body.

Let $A = G_{ve}/\eta_{ve}$. Equation (5) can be transformed into

$$\varepsilon_{ve} = \frac{\sigma_1 - \sigma_3}{3G_{ve}}\left[1 - \exp\left(-At\right)\right]. \tag{6}$$

Therefore, the viscoelastic strain rate can be obtained as

$$\varepsilon'_{ve} = A \cdot \frac{\sigma_1 - \sigma_3}{3G_{ve}} \cdot \exp(-At) \tag{7}$$

Equation (8) is obtained by combining Eqs. (6) and (7).

$$\left(A\varepsilon_{ve} + \varepsilon'_{ve}\right) \exp(-At) = \varepsilon'_{ve}. \tag{8}$$

Equation (9) is obtained using the Taylor series to expand the exponential function in Eq. (8).

$$\exp(-At) = 1 - At + (At)^2 + o\left(t^3\right). \tag{9}$$

Equation (10) is obtained by substituting Eq. (9) into Eq. (8).

$$\left(A\varepsilon_{ve} + \varepsilon'_{ve}\right)\left[1 - At + (At)^2\right] = \varepsilon'_{ve}. \tag{10a}$$

The relationship between viscoelastic strain and viscoelastic strain rate is obtained by simplifying Eq. (10a).

$$\varepsilon_{ve}t^2A^3 + \left(\varepsilon'_{ve}t^2 - \varepsilon_{ve}t\right)A^2 + \left(\varepsilon_{ve} - \varepsilon'_{ve}t\right)A = 0. \tag{10b}$$

According to the root-finding equation of the cubic equation in one variable, parameter A can be obtained. In Eq. (10b), the viscoelastic strain and the viscoelastic strain rate are taken at different points in time. The value of parameter A is also different. The value of parameter A is time sensitive. Different points in time have corresponding parameter A values. The shear modulus G_{vei} can be determined at different points in time by substituting parameter A into Eq. (6) (Hamza et al. 2018; Yoshida et al. 1992).

$$G_{vei} = \frac{\sigma_1 - \sigma_3}{3\varepsilon_{vei}}\left[1 - \exp\left(-A_i t_i\right)\right]. \tag{11}$$

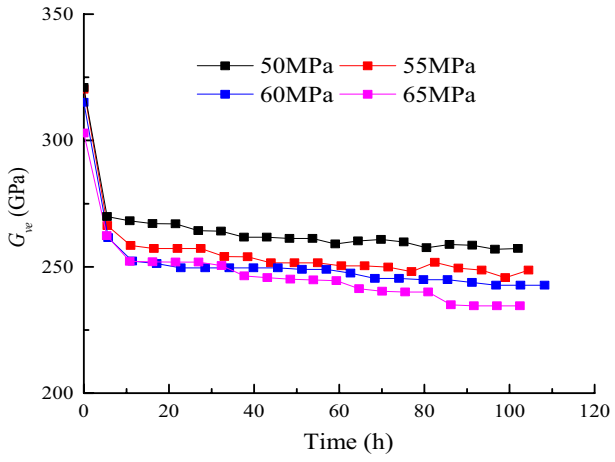

Fig. 8 Shear modulus at different time points under different axial stresses

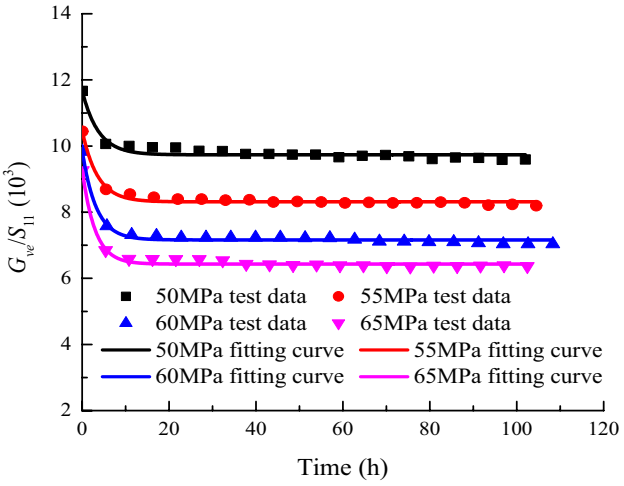

Fig. 9 Shear modulus under different stresses under different axial stresses at different times

The viscosity coefficient can be obtained by substituting the calculated shear modulus G_{vei} into A.

$$\eta_{vei} = \frac{G_{vei}}{a_i}, \tag{12}$$

where G_{vei} is the shear modulus at any time, η_{vei} is the viscosity coefficient at any time, A_i is the value of the parameter A at any time, and t_i is the different time point.

Through the above equations, the viscosity coefficient and shear modulus can be calculated at any time. The change of viscosity coefficient and shear modulus at any time is drawn as shown in Fig. 8 (Riva et al. 2018; Xu et al. 2018a). Figure 8 shows that the viscosity coefficient and the shear modulus first decrease and then reach stable. The viscosity coefficient and shear modulus at the same time point also decrease trend with the increase of stress. This finding shows that the viscoelastic creep parameters deteriorate with time and stress.

In the present study, the viscoelastic creep parameters and stress and time presumably satisfy the following relationship to describe the influence of stress and time on the change of viscoelastic creep parameters (Yang et al. 2021).

Table 2 The fitting parameters of the shear modulus G_{ve}

Fitting parameters Stress level/MPa	50 MPa	55 MPa	60 MPa	65 MPa
a_2	9.735	8.313	7.161	6.430
b_2	1.942	2.155	2.709	2.879
c_2	3.730	3.527	3.220	2.927
R^2	0.906	0.952	0.932	0.976

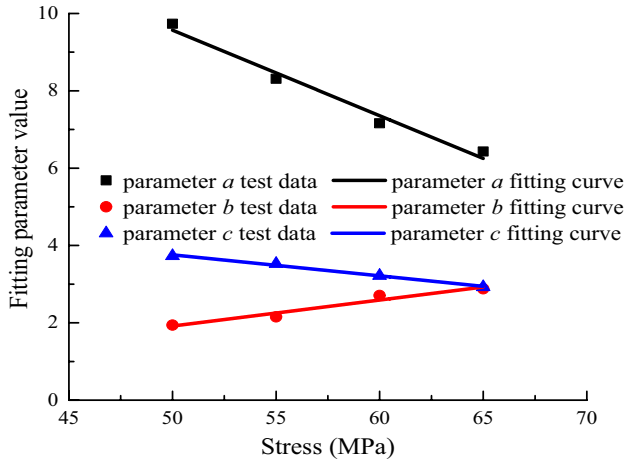

Fig.10 The relationship between fitting parameters and stress

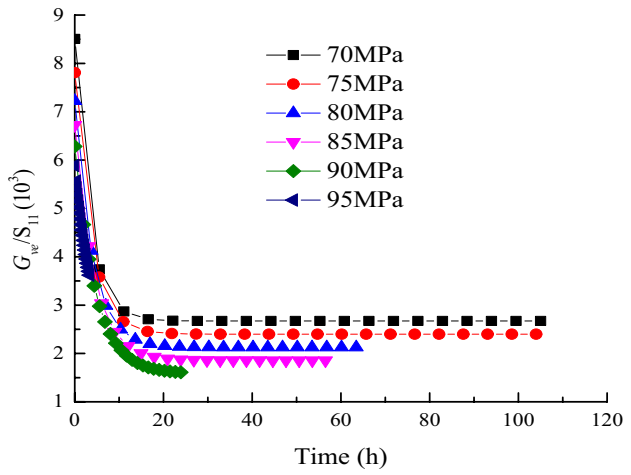

Fig. 11 Shear modulus under other stress levels under different stresses at different points in time

$$\left(G_{ve}, \eta_{ve}\right) = g\left[S_{11}, t\right], \tag{13}$$

where $g(\cdot)$ is a function. The calculation of S_{11} here can be seen in Eq. (3c).

The change of shear modulus under different values of stress and time can be drawn, as shown in Fig. 9.

The expressions of stress and time, shear modulus, and viscosity coefficient can be obtained by using the form of Eq. (13) to fit the changing shear modulus.

$$\frac{G_{ve}}{S_{11}} = a_2 \exp\left(-\frac{t}{b_2}\right) + c_2 \tag{14}$$

$$\frac{\eta_{ve}}{S_{11}} = a_3 \exp\left(-\frac{t}{b_3}\right) + c_3, \tag{15}$$

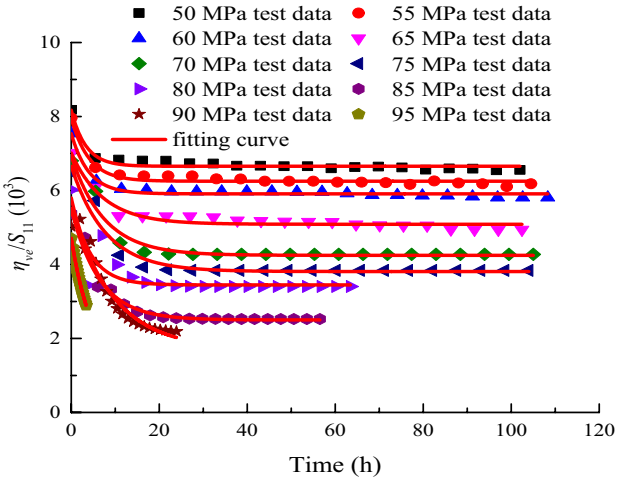

Fig. 12 Viscosity coefficient under different stresses at different points in time

Table 3 Fitting parameter values of the viscosity coefficient under different stresses and different time points

Stress level/MPa Fitting parameters	a_3	b_3	c_3	R^2
50	6.654	1.516	3.304	0.944
55	6.251	1.697	4.032	0.958
60	5.909	1.628	3.984	0.968
65	5.087	1.927	7.306	0.939
70	4.247	2.681	7.478	0.952
75	3.809	2.846	7.817	0.950
80	3.446	2.354	4.281	0.921
85	2.500	3.006	6.400	0.976
90	1.700	3.806	9.715	0.949
95	1.050	3.660	4.944	0.987

where a_2, b_2, c_2, a_3, b_3, and c_3 are the fitting parameters.

The specific values of the fitting parameters are shown in Table 2.

The relationship between fitting parameters and stress are shown in Fig. 10. The relationship between each fitting parameter and stress are

$$\begin{cases} a_2 = 121.281 \exp\left(-\sigma_1/16.174\right) + 4.233, R^2 = 0.998 \\ b_2 = 0.067\sigma_1 - 1.447, R^2 = 0.904 \\ c_2 = -0.054\sigma_1 + 6.476, R^2 = 0.987 \end{cases}, \tag{16}$$

where σ_1 is the axial stress.

The shear modulus G_{ve} of the viscoelastic body under other stress levels can be calculated by substituting this

parameter value into Eq. (14). The shear modulus G_{ve} of the viscoelastic body under other stress levels is shown in Fig. 11.

The viscosity coefficient of the viscoelastic body under different stresses and different time points is calculated by using Eq. (12) as well as the shear modulus of the viscoelastic body under different stresses and time points. The viscosity coefficient under different stresses at different points in time is shown in Fig. 12. The fitting parameter values of the viscosity coefficient of the viscoelastic body are shown in Table 3.

Figures 9, 10, 11 and 12 show that as the time increases, the viscoelastic shear modulus and viscoelastic viscous coefficient of the rock first decrease and then become stable. The viscoelastic shear modulus and viscoelastic viscous coefficient of the rock also decrease with the continuous increase of stress. This finding shows that the viscoelastic creep parameters of the rocks constantly degrade under the dual effects of time and stress.

3.4 Establishment of the Viscoplastic Strain Model

The instantaneous strain, viscoelastic strain and viscoplastic strain of the creep curve are separated by the method in Sect. 3. The relationship between instantaneous strain, viscoelastic strain and viscoplastic strain with stress and time are established. The relationship between creep parameters and time and stress are analyzed.

In a three-dimensional stress state, the creep equation of Newton's dashpot is (Wang et al. 2016)

$$\varepsilon_{vp} = \frac{\sigma_1 - \sigma_3 - \sigma_s}{3\eta_{vp}} t, \tag{17}$$

where ε_{vp} is the strain of the Newton 's dashpot, and η_{vp} is the viscosity coefficient of the Newton 's dashpot.

For a three-dimensional stress state, the viscosity coefficient of Newton's dashpot can be directly determined by Eq. (17).

$$\eta_{vp} = \frac{\sigma_1 - \sigma_3 - \sigma_s}{3\varepsilon_{vp}} t. \tag{18}$$

The Newton's dashpot cannot describe the accelerated creep of rock. Therefore, this paper refers to the non-linear dashpot to describe the accelerated creep of rock. Under a three-dimensional stress state, the creep equation of the non-linear dashpot is Eq. (1a) (Qi et al. 2012).

In this paper, the non-linear dashpot in series with Newton 's dashpot is used to describe the viscoplastic strain change with accelerated creep. The model equation of non-linear dashpot in series with Newton 's dashpot is

$$\varepsilon_{vpnl} = \frac{\sigma_1 - \sigma_3 - \sigma_s}{3\eta_{vp}} t + \frac{\sigma_1 - \sigma_3}{6\eta_{nl}} (t - t^*)^2. \tag{19}$$

The viscoplastic strain rate can be obtained by taking the first derivative with respect to time of Eq. (19).

$$\varepsilon'_{vpnl} = \frac{\sigma_1 - \sigma_3 - \sigma_s}{3\eta_{vp}} + \frac{\sigma_1 - \sigma_3}{3\eta_{nl}} (t - t^*). \tag{20}$$

The viscosity coefficient η_{vp} can be obtained by combining Eqs. (19) and (20).

$$\eta_{vp} = \frac{(\sigma_1 - \sigma_3)(t - t^*) - 2(\sigma_1 - \sigma_3 - \sigma_s)t}{3\left[\varepsilon'_{vpnl}(t - t^*) - 2\varepsilon_{vpnl}\right]}. \tag{21}$$

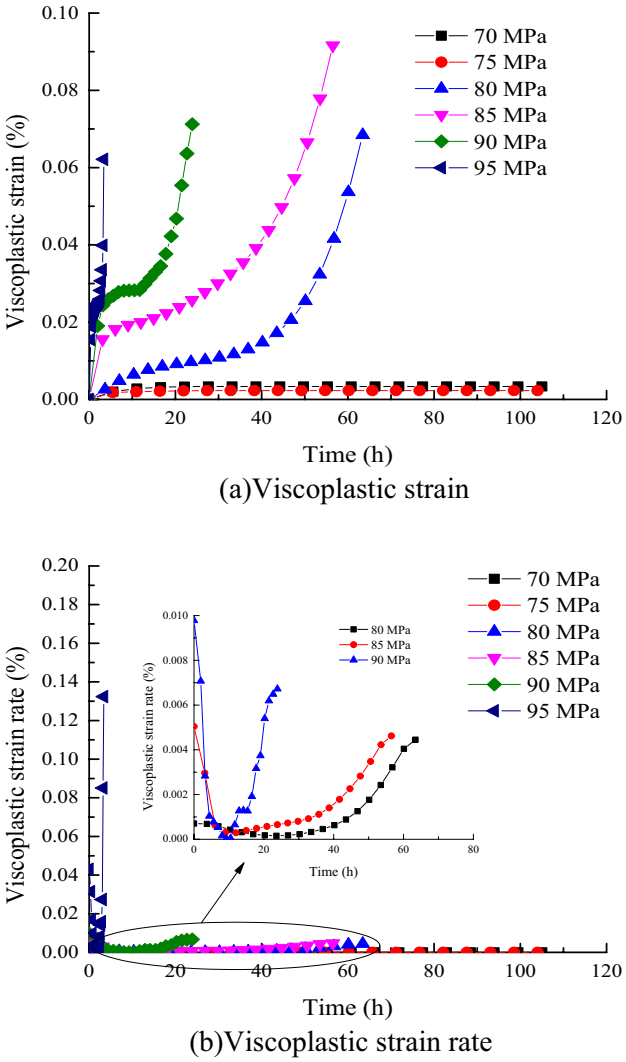

Fig. 13 Viscoplastic strain and viscoplastic strain rateunder different stresses at different points in time

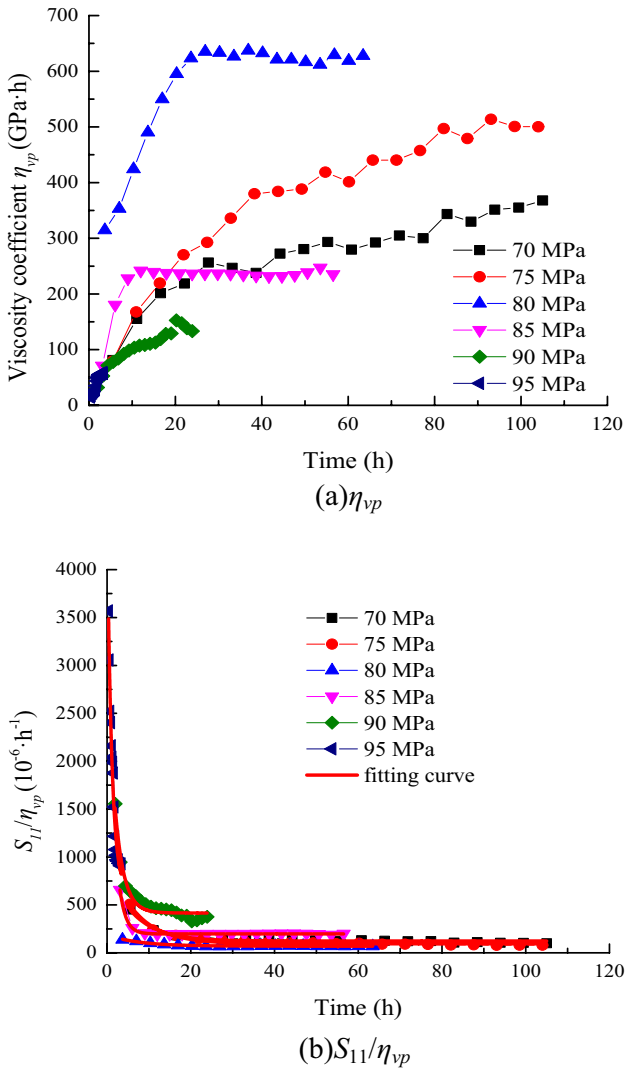

Fig. 14 The variation of the viscosity coefficient of Newton's dashpot under different stresses at different points in time

The viscosity coefficient η_{nl} can be obtained by substituting the viscosity coefficient η_{vp} into Eq. (20).

$$\eta_{nl} = \frac{(\sigma_1 - \sigma_3)(t - t^*)}{3\eta_{vp}\varepsilon'_{vpnl} - (\sigma_1 - \sigma_3 - \sigma_s)}\eta_{vp}. \tag{22}$$

The viscoplastic strain of rock can be expressed as

$$\varepsilon_{vpnl} = \varepsilon - \varepsilon_e - \varepsilon_{ve}. \tag{23}$$

The shear modulus G_{ve} and viscosity coefficient η_{ve} of the viscoelastic body under different stresses can be calculated by substituting the stress values into Eqs. (14), and (15). The viscoelastic strain values of the rock under different stresses can be obtained by substituting the shear modulus G_{ve} and viscosity coefficient η_{ve} of the viscoelastic body under different stresses in Eq. (4) (Liu et al. 2019). The viscoplastic strain and viscoplastic strain rate of the rock are obtained by substituting the viscoelastic strain values under different stresses into Eq. (23), as shown in Fig. 13.

Table 4 Fitting parameters of the viscosity coefficient of Newton's dashpot under different stresses at different points in time

Stress level/MPa Fitting parameters	a_4	b_4	c_4	R^2
70	767.346	6.358	123.392	0.957
75	907.989	6.725	94.034	0.975
80	119.830	7.386	69.299	0.969
85	3741.005	1.471	197.118	0.999
90	2741.177	2.113	415.702	0.959
95	3955.808	1.087	645.262	0.973

Equation (21) calculates the viscosity coefficient η_{vp} of the Newton 's dashpot under different stresses. The variation of the viscosity coefficient of Newton's dashpot under different stresses are shown in Fig. 14.

Figure 14 shows that $S_{11}/\eta_{vp}(S_{11})$ controls the viscoplastic creep of the rock. As time increases, it gradually decreases and tends to a stable value. $\eta_{vp}(S_{11})$ increases with time and shows a pattern of first changing and then becoming stable. In particular, the sample has entered the steady-state creep stage.

Equation (25) fits the variation the viscosity coefficient of Newton's dashpot. The expressions of stress and time and the viscosity coefficient of Newton's dashpot can be obtained.

$$\frac{\eta_{vp}}{S_{11}} = a_4 \exp\left(-\frac{t}{b_4}\right) + c_4, \tag{25}$$

where a_4, b_4, and c_4 are the fitting parameters.

The fitting parameter values of the viscosity coefficient of Newton's dashpot under the action of different stresses and at different points in time are shown in Table 4.

Equation (22) calculates the viscosity coefficient η_{nl} of the non-linear dashpot under different stresses. The viscosity coefficient of the non-linear dashpot under different stresses are shown in Fig. 15.

Figure 15 shows that as the time increases, the viscosity coefficient of the non-linear dashpot under different stresses shows increase first and then remains constant. As time increases, S_{11}/η_{nl} under different stresses first decrease and then remains constant. However, the change of S_{11}/η_{nl} under the action of the same time is increasing.

The variation of the viscosity coefficient of the non-linear dashpot is fitted by the form of Eq. (26). The expressions of

stress and time and viscosity coefficient of non-linear dashpot can be obtained.

$$\frac{\eta_{nl}}{S_{11}} = a_5 \exp\left(-\frac{t}{b_5}\right) + c_5, \tag{26}$$

where a_5, b_5, and c_5 are the fitting parameters.

The fitting parameter values of the non-linear dashpot's viscosity coefficient under the action of different stresses and different time points are shown in Table 5.

4 Establishment and Verification of the Creep Model

The traditional creep model can describe the instantaneous, viscoelastic, and viscoplastic strains after the instantaneous, viscoelastic, and viscoplastic strains of the creep curve are separated. A method to determine the creep parameters is also obtained (Zhao et al. 2018). The relationship between creep parameters and time and stress are analyzed, and the expression between creep parameters and time and stress is constructed. Finally, the series–parallel rule can be used to superimpose the above mentioned traditional creep models describing the instantaneous, viscoelastic, and viscoplastic strains and obtain a creep model considering the deterioration of creep parameters.

By substituting Eqs. (3a), (3b), (14), (25) and (26) into Eqs. (1b)–(1d), the improved creep model can be obtained as follows.

When $\sigma < \sigma_A$ and $\varepsilon < \varepsilon_a$,

$$\varepsilon = \frac{\sigma_1 + 2\sigma_3}{9K_e(\sigma_m, t)} + \frac{\sigma_1 - \sigma_3}{3G_e(\sigma_1)} + \frac{\sigma_1 - \sigma_3}{3G_{ve}(S_{11}, t)}\left[1 - \exp\left(-\frac{G_{ve}(S_{11}, t)}{\eta_{ve}(S_{11}, t)}t\right)\right] \tag{27}$$

When $\sigma \geq \sigma_A$, $\sigma < \sigma_S$ and $\varepsilon < \varepsilon_a$,

$$\varepsilon = \frac{\sigma_1 + 2\sigma_3}{9K_e(\sigma_m, t)} + \frac{\sigma_1 - \sigma_3}{3G_e(\sigma_1)} + \frac{\sigma_1 - \sigma_3}{3G_{ve}(S_{11}, t)}\left[1 - \exp\left(-\frac{G_{ve}(S_{11}, t)}{\eta_{ve}(S_{11}, t)}t\right)\right] + \frac{\sigma_1 - \sigma_3 - \sigma_s}{3\eta_{vp}(S_{11}, t)}t \tag{28}$$

When $\sigma \geq \sigma_S$ and $\varepsilon \geq \varepsilon_a$,

$$\varepsilon = \frac{\sigma_1 + 2\sigma_3}{9K_e(\sigma_m, t)} + \frac{\sigma_1 - \sigma_3}{3G_e(\sigma_1)} + \frac{\sigma_1 - \sigma_3}{3G_{ve}(S_{11}, t)}\left[1 - \exp\left(-\frac{G_{ve}(S_{11}, t)}{\eta_{ve}(S_{11}, t)}t\right)\right] + \frac{\sigma_1 - \sigma_3 - \sigma_s}{3\eta_{vp}(S_{11}, t)}t + + \frac{\sigma_1 - \sigma_3}{6\eta_{nl}(S_{11}, t)}(t - t^*)^2. \tag{29}$$

By substituting the expression of creep parameters under different time and stress into the Eqs. (27)–(29), the creep model curve considering the deterioration of creep parameters can be obtained. The comparison between the model curve and the test curve can be shown in Fig. 16.

Figure 16 shows that the model can clearly describe the whole process of creep. It makes up for the shortcoming that the traditional Nishihara creep model cannot describe the accelerated creep. Therefore, the construction process of the model is correct and reasonable. The model can truly reflect the creep and stress state of sandstone. It also has guiding relevance for solving the long-term stability of the surrounding rock in practical engineering.

5 Discussion

5.1 Further Verification

The comparison of the traditional Nishihara model curve, the model curve in this study, and the test curve can be shown in Fig. 17 (taking the confining pressure of 15 MPa as an example, the Nishihara model curve, the test curve and the model curve of this paper are analyzed).

The creep model established in this paper can well describe the whole process of creep. It can also make up for the deficiency that the traditional creep models cannot describe the characteristics of accelerated creep. Therefore, the method to separate viscoelastic and viscoplastic strains can be considered correct and reasonable.

5.2 Understanding the Separation of Viscoelastic Strain and Viscoplastic Strain

In deep geological environments, hard rock has a distinct stress threshold (long-term rock strength) during creep. The rock hardening effect is stronger than the damage effect when the stress is less than the threshold. The fissures

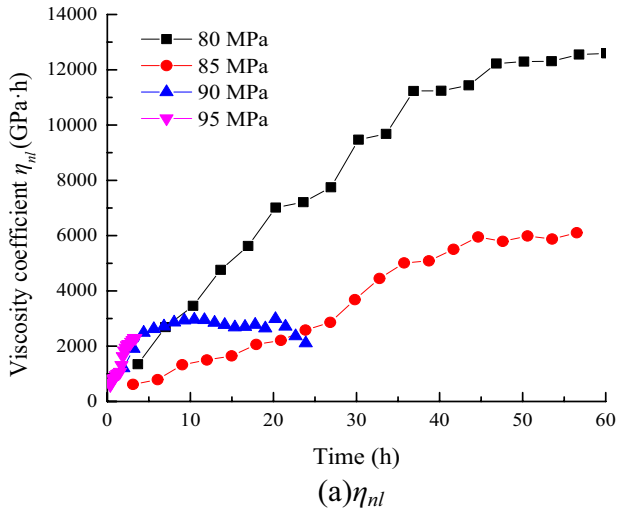

(a)η_{nl}

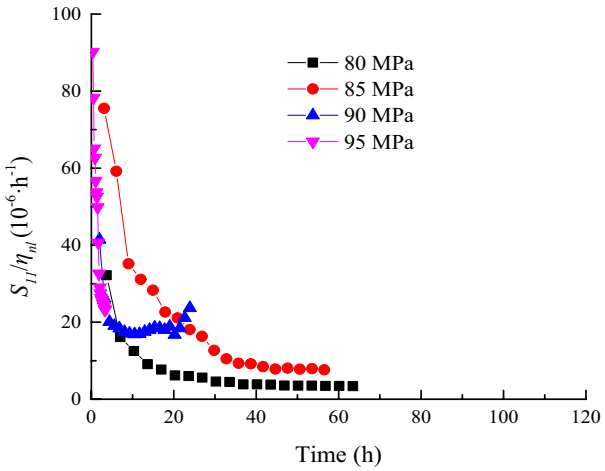

(b)S_{11}/η_{nl} test data

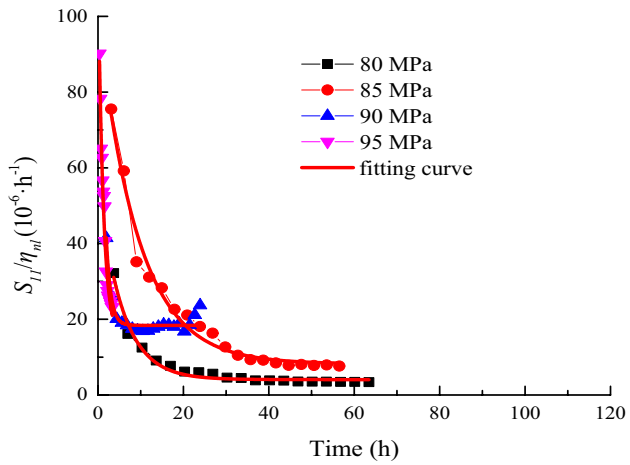

(c)S_{11}/η_{nl} fitting curve

Fig. 15 The variation of viscosity coefficient of non-linear dashpot under different stresses at different points in time

Table 5 Fitting parameter values of the non-linear viscous pot's viscosity coefficient under different stresses and different time points

Stress level/MPa Fitting parameters	a_5	b_5	c_5	R^2
80	52.83726	5.49786	4.06086	0.97869
85	92.04141	9.29277	8.20398	0.97938
90	145.73506	1.05613	18.38333	0.90801
95	98.26091	1.2238	14.88573	0.97327

generated by the intergranular cement under the action of external force gradually close with the rock particle flow. After the external force is withdrawn, the deformation of the particle body can be restored immediately. The relative

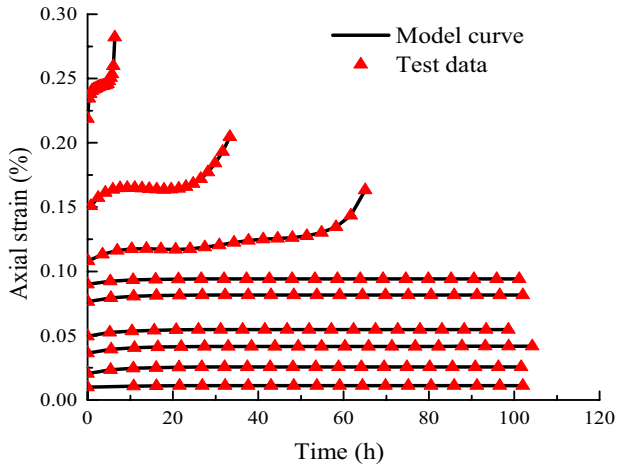

(a)10MPa

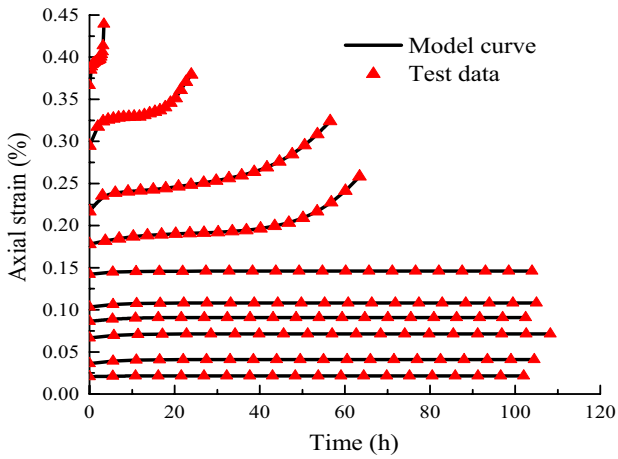

(b)15MPa

Fig. 16 Comparison between test curve and improved creep model curve

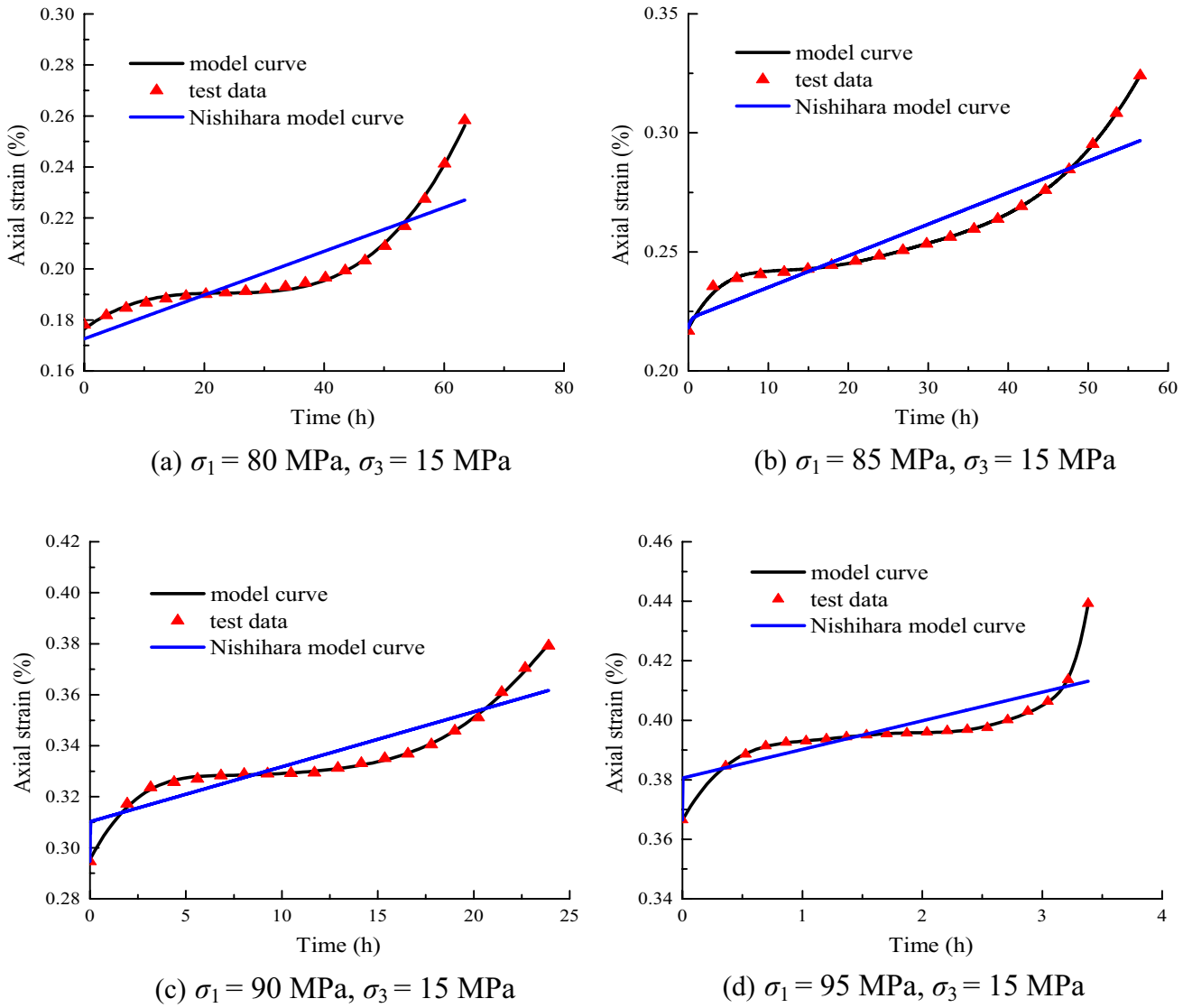

Fig. 17 Comparison of the traditional Nishihara model curve, the model curve derived in this study, and the test curve

displacement between particles recovers slowly with time. The instantaneous elastic and viscoelastic characteristics of the rock creep are exhibited macroscopically. The rock damage effect is stronger than the hardening effect when the stress exceeds the threshold. The cracks between the rock particles gradually develop under the action of external force. This will lead to the local damage of the rock particles. The deformation of the particle body can be restored immediately when the external force is withdrawn. The undamaged part of the interparticle cement gradually recovers with time, but the damaged part cannot be recovered (Liu et al. 2020). It shows the instantaneous elasticity, viscoelasticity, and viscoplastic characteristics of rock creep on the macroscopic scale. In the past creep tests, the viscoelastic and viscoplastic strains of the rock are obtained. However, separating the creep curve into viscoelastic strain and viscoplastic strain curve can be not involved. It is impossible to reveal the creep failure mechanism of rock. Therefore, the instantaneous elasticity, viscoelasticity, and viscoplastic creep of rock creeps are studied separately. This will lay a good foundation for subsequent model building and numerical calculation (Fan et al. 2010).

Separating the viscoelastic and viscoplastic creeps of the rock creep and conducting quantitative analysis are necessary to study the creep of rock under high stress (Zhao et al. 2017b). For intact rocks, the viscoelastic creep can be a function of stress. A functional relationship between rock viscoelastic strain and stress at low stress levels are established. This functional relationship is used to derive the viscoelastic strain at high stress levels. The viscoplastic

creep of the rock is obtained by substituting it into Eq. (23). Therefore, instantaneous elastic, viscoelastic, and viscoplastic strains must be fitted separately. It can fully consider the viscoplastic strain in the decaying creep stage. It can obtain the real parameter variation in the accelerated creep stage. The established creep model can effectively reflect the nonlinear characteristics of the rock creep.

6 Conclusions

The rock creep strain can be separated into viscoelastic and viscoplastic strains. According to the degradation of creep parameters, the instantaneous elastic parameters, viscoelastic parameters, viscoplastic parameters, and functions of time and stress are established under stress and time. The improved model can effectively reflect the non-linear characteristics of the whole process of rock creep. It also considers instantaneous, viscoelastic, and viscoplastic strains. The model curve is highly consistent with the test curve. The comparison results verify that the creep model established in this study can be reasonable and feasible.

The shear modulus G_e in the instantaneous strain stage is degraded under stress. The bulk modulus K_e is reflected in the change from a positive value to a negative value. The rock is in a state of expansion when the stress is greater than 80 MPa. However, the absolute value of K_e decreases. As time increases, the viscoelastic shear modulus G_{ve} and viscoelastic viscous coefficient η_{ve} of the rock first decrease and then remains constant.

The ratio of stress tensor to viscosity coefficient S_{11}/η_{vp} controls the viscoplastic creep of the rock. The viscosity coefficient η_{vp} increases with time and first increases and then remains constant. As time increases, the change of S_{11}/η_{nl} under different stresses shows a trend of first decreasing and then becoming stable.

Acknowledgements This work was supported by the National Natural Science Foundation of China (Grant nos. 4206070032 and 41941018), the Science and Technology Service Network Initiative of the Chinese Academy of Sciences (Grant no. KFJSTS-QYZD-174), and the Guangxi Natural Science Foundation (Grant no. 2020GXNSFAA159125).

Author contributions WL: conceptualization, data curation, writing—original draft, investigation, and methodology. HZ: conceptualization, writing—original draft, writing—review and editing, software, supervision, and methodology. SZ: conceptualization, data curation, methodology, and investigation. CZ: English grammar correction and language polishing, supervision and writing—review and editing.

Data availability The datasets used in this study are available upon reasonable request from the corresponding author.

Declarations

Conflict of interest The authors declared that they have no conflicts of interest to this work.

References

Andargoli MBE, Shahriar K, Ramezanzadeh A, Goshtasbi K (2019) The analysis of dates obtained from long-term creep tests to determine creep coefficients of rock salt. Bull Eng Geol Environ 78(3):1617–1629

Brantut N, Heap MJ, Meredith PG (2013) Time-dependent cracking and brittle creep in crustal rocks: a review. J Struct Geol 52:17–43

Cornet JS, Dabrowski M (2018) Non-linear viscoelastic closure of salt cavities. Rock Mech Rock Eng 51(10):3091–3109

Diisterloh U, Lerche S, Lux KH (2013) Damage and healing properties of rock salt: long-term cyclic loading tests and numerical back analysis//Clean energy systems in the subsurface: production, storage and conversion. Springer, Berlin, pp 341–362

Fan QY, Yang KQ, Wang WM (2010) Study on creep mechanism of muddy soft rock. Chin J Rock Mech Eng 29(8):1555–1561 ((**in Chinese**))

Findley WN, Lai JS, Onaran K (1976) Creep and relaxation of nonlinear viscoelastic materials with an introduction to linear viscoelasticity. North Holland, Amsterdam

Hamza O, Stace R (2018) Creep properties of intact and fractured muddy siltstone. Int J Rock Mech Min Sci 106:109–116

Heap MJ, Baud P, Meredith PG (2009) Time-dependent brittle creep in Darley Dale sandstone. J Geophys Res Solid Earth 114:B07203

Hou RB, Zhang K, Tao J, Xue XR, Chen YL (2019) A non-linear creep damage coupled model for rock considering the effect of initial damage. Rock Mech Rock Eng 52(5):1275–1285

Hu B, Yang SQ, Xu P (2018) A non-linear rheological damage model of hard rock. J Cent South Univ 25(7):1665–1677

Huang M, Liu XR (2011) Study on the relationship between parameters of deterioration creep model of rock under different modeling assumptions//Advanced materials research. Trans Tech Publ Ltd 243:2571–2580

Jin J, Cristescu ND (1998) An elastic/viscoplastic model for instantaneous creep of rock salt. Int J Plast 14(1–3):85–107

Jing W, Zhao Y, Kong J, Huang C, Jilani KM, Li H (2018) The time-space prediction model of surface settlement for above underground gas storage cavern in salt rock based on Gaussian function. J Nat Gas Sci Eng 53:45–54

Li WQ, Li XD, Han B, Shu Y (2007) Recognition of creep model of layer composite rock mass and its application. J Cent South Univ Technol 14(1):329–331

Liu WB, Zhang SG (2021) An improved unsteady creep model based on the time dependent mechanical parameters. Mech Adv Mater Struct 28(17):1838–1848

Liu XX, Li SN, Xu ZP, Li Y, Gao XW, Wang WW (2019) Viscoelastic-plastic creep model of high stress argillaceous siltstone. J Cent South Univ Sci Technol 50(5):1210–1220 ((**in Chinese**))

Liu XX, Li SN, Zhou YM, Li Y, Wang WW (2020) Study on creep behavior and long-term strength of argillaceous siltstone under high stresses. Chin J Rock Mech Eng 39(1):138–146 ((**in Chinese**))

Liu WB, Zhou H, Zhang SG, Jiang S, Yang L (2022) A non-linear creep model for surrounding rocks of tunnels based on kinetic energy theorem. J Rock Mech Geotech Eng 55(2):363–374

Ma LJ, Liu XY, Fang Q, Xu HF, Xia HM, Li EB, Li WP (2013) A new elasto-viscoplastic damage model combined with the generalized Hoek-Brown failure criterion for bedded rock salt and its application. Rock Mech Rock Eng 46(1):53–66

Munson DE, Weatherby JR (1993) Two- and three-dimensional calculations of scaled in situ tests using the M-D model of salt creep. Int J Rock Mech Min Sci Geomech Abstr 30(7):1345–1350

Qi YJ, Jiang QH, Wang ZJ (2012) 3D creep constitutive equation of modified Nishihara model and its parameters identification. Chin J Rock Mech Eng 31(2):347–355

Riva F, Agliardi F, Amitrano D, Crosta GB (2018) Damage-based time-dependent modeling of paraglacial to postglacial progressive failure of large rock slopes. J Geophys Res Earth Surf 123(1):124–141

Shen MR, Chen HJ (2011a) Testing study of long-term strength characteristics of red sandstone. Rock Soil Mech 32(11):3301–3305

Singh A, Kumar C, Kannan LG, Rao KS, Ayothiraman R (2018) Estimation of creep parameters of rock salt from uniaxial compression tests. Int J Rock Mech Min Sci 107:243–248

Tang H, Wang D, Huang R, Pei X, Chen W (2018) A new rock creep model based on variable-order fractional derivatives and continuum damage mechanics. Bull Eng Geol Environ 77(1):375–383

Tomanovic Z (2006) Rheological model of soft rock creep based on the tests on marl. Mech Time Dependent Mater 10(2):135–154

Wang J, Liu X, Song Z, Guo J, Zhang Q (2016) A creep constitutive model with variable parameters for thenardite. Environ Earth Sci 75(11):1–12

Wang R, Jiang Y, Yang C, Huang F, Wang Y (2018a) A non-linear creep damage model of layered rock under unloading condition. Math Probl Eng 20:18

Wang X, Yin Y, Wang J, Lian B, Qiu H, Gu T (2018b) A nonstationary parameter model for the sandstone creep tests. Landslides 15(7):1377–1389

Wu F, Liu JF, Wang J (2015) An improved Maxwell creep model for rock based on variable-order fractional derivatives. Environ Earth Sci 73(11):6965–6971

Xu M, Jin D, Song E, Shen D (2018a) A rheological model to simulate the shear creep behavior of rockfills considering the influence of stress states. Acta Geotech 13(6):1313–1327

Xu T, Zhou G, Heap MJ, Yang S, Konietzky H, Baud P (2018b) The modeling of time-dependent deformation and fracturing of brittle rocks under varying confining and pore pressures. Rock Mech Rock Eng 51(10):3241–3263

Xu T (2015) Creep model of brittle rock and its application to rock slope stability. In: International symposium on mega earthquake induced geo-disasters and longterm effects

Yan Y (2009) Research on rock creep tests under seepage flow and variable parameters creep equation, PHD. Tsinghua University, Beijing

Yan Y, Wang SJ, Wang EZ (2010) Creep equation of variable parameters based on Nishihara model. Rock Soil Mech 31(10):3025–3035 ((**in Chinese**))

Yang L, Li ZD (2018) non-linear variation parameters creep model of rock and parametric inversion. Geotech Geol Eng 36(5):2985–2993

Yang X, Jiang A, Zhang F (2021) Research on creep characteristics and variable parameter-based creep damage constitutive model of gneiss subjected to freeze–thaw cycles. Environ Earth Sci 80(1):1–16

Yoshida H, Horii H (1992) A micromechanics-based model for creep behavior of rock. Appl Mech Rev 45(8):294–303

Yu M, Mao X, Hu X (2016) Shear creep characteristics and constitutive model of limestone. Int J Min Sci Technol 26(3):423–428

Zhang L (2021) Theoretical and experimental research on the evolution of creep-seepage for coal containing gas. China University of Mining and Technology, Beijing ((**in Chinese**))

Zhang SG, Liu WB, Chen L (2019) Unsteady creep model based on time-dependentness of mechanical parameters. J China Univ Min Technol 48(5):993–1002

Zhao YL, Wang YX, Wang WJ, Wan W, Tang JZ (2017a) Modeling of non-linear rheological behavior of hard rock using triaxial rheological experiment. Int J Rock Mech Min Sci 93:66–75

Zhao YL, Zhang LY, Wang WJ, Wan WW, Li SQ, Ma WH, Wang YX (2017b) Creep behavior of intact and cracked limestone under multi-level loading and unloading cycles. Rock Mech Rock Eng 50(6):1409–1424

Zhao YL, Zhang LY, Wang WJ, Wan WW, Ma WH (2018) Separation of elastoviscoplastic strains of rock and a non-linear creep model. Int J Geomech 18(1):04017129

Zhou W, Chang XL, Zhou CB, Liu XH (2010) Creep analysis of high concrete-faced rockfill dam. Int J Numer Methods Biomed Eng 26(11):1477–1492

Zhou HW, Wang CP, Han BB, Duan ZQ (2011) A creep constitutive model for salt rock based on fractional derivatives. Int J Rock Mech Min Sci 48(1):116–121